⌘ *Author's Choice*

THE JOURNAL OF BIOLOGICAL CHEMISTRY VOL. 284, NO. 21, pp. 14337–14346, May 22, 2009

Real-time Analysis of Conformation-sensitive Antibody Binding Provides New Insights into Integrin Conformational Regulation*[S]

Received for publication, February 19, 2009 Published, JBC Papers in Press, February 27, 2009, DOI 10.1074/jbc.M901178200

Alexandre Chigaev[‡§1], Anna Waller[§], Or Amit[§], Liliana Halip[¶‖], Cristian G. Bologa[¶], and Larry A. Sklar[‡§2]

From the [‡]Department of Pathology, [§]Cancer Research and Treatment Center, and [¶]Department of Biochemistry and Molecular Biology, University of New Mexico Health Sciences Center, Albuquerque, New Mexico 87131 and the [‖]Institute of Chemistry, Romanian Academy, Timisoara 300223, Romania

Integrins are heterodimeric adhesion receptors that regulate immune cell adhesion. Integrin-dependent adhesion is controlled by multiple conformational states that include states with different affinity to the ligand, states with various degrees of molecule unbending, and others. Affinity change and molecule unbending play major roles in the regulation of cell adhesion. The relationship between different conformational states of the integrin is unclear. Here we have used conformationally sensitive antibodies and a small LDV-containing ligand to study the role of the inside-out signaling through formyl peptide receptor and CXCR4 in the regulation of $\alpha_4\beta_1$ integrin conformation. We found that in the absence of ligand, activation by formyl peptide or SDF-1 did not result in a significant exposure of HUTS-21 epitope. Occupancy of the ligand binding pocket without cell activation was sufficient to induce epitope exposure. EC_{50} for HUTS-21 binding in the presence of LDV was identical to a previously reported ligand equilibrium dissociation constant at rest and after activation. Furthermore, the rate of HUTS-21 binding was also related to the VLA-4 activation state even at saturating ligand concentration. We propose that the unbending of the integrin molecule after guanine nucleotide-binding protein-coupled receptor-induced signaling accounts for the enhanced rate of HUTS-21 binding. Taken together, current results support the existence of multiple conformational states independently regulated by both inside-out signaling and ligand binding. Our data suggest that VLA-4 integrin hybrid domain movement does not depend on the affinity state of the ligand binding pocket.

In the bloodstream circulating leukocytes respond to inflammatory signals by rapid changes of cell adhesive properties. These include cell tethering, rolling, arrest, and firm adhesion, all of which are well described steps of leukocyte recruitment to the sites of inflammation (1). Leukocyte arrest and firm adhesion are mediated exclusively by integrin receptors (2). At the same time integrins can also mediate tethering and rolling (3). These largely diverse cell adhesive properties are achieved by sophisticated conformational regulation; multiple states of the same molecule with different affinity for its ligand and different degrees of molecular unbending are attributed to various types of "cellular behavior." It is proposed that the low affinity bent state translates into a non-adhesive resting cell, the low affinity unbent or extended state of integrin results in cell rolling, and the high affinity state promotes cell arrest (4, 5). However, the exact sequence of conformational events and the relationship between integrin conformational and functional activity remain key questions (6).

Integrin conformation is regulated through G-protein-coupled receptors by a signaling pathway which is initiated by ligand binding to a GPCR,[3] propagated inside the cell, and results in the binding of signaling proteins (such as talin and others) to cytoplasmic domains of integrin subunits. This binding leads to a separation of the integrin cytoplasmic domains and inside-out activation (6). Chemokines (chemotactic cytokines) as well as "classical" chemoattractants (such as formyl peptide) preferentially signal through heterotrimeric G-proteins coupled to the $G\alpha_i$ subunit (1). Activation by these ligands results in up-regulation of integrin affinity and/or conformational unbending (extension) of the integrin molecule. These conformational changes lead to cell arrest and firm adhesion. G-protein receptors coupled to $G\alpha_s$-coupled subunit (adenylyl cyclase/cAMP signaling pathway) can actively down-regulate the affinity state of the ligand binding pocket without changing integrin conformational unbending. This provides an anti-adhesive signal and results in cell de-adhesion (7). Thus, interac-

* This work was supported, in whole or in part, by National Institutes of Health Grants HL56384 and HL081062 (to L. A. S.). This work was also supported by Leukemia and Lymphoma Society Grant 7388-06 (to L. A. S.) and by Dedicated Health Research Funds of the University of New Mexico School of Medicine Grant C-2297-RAC (to A. C.).

⌘ *Author's Choice*—Final version full access.

[S] The on-line version of this article (available at http://www.jbc.org) contains supplemental structures shown in Fig. 6.

[1] To whom correspondence may be addressed: MSC08 4630, 915 Camino de Salud, Albuquerque, NM 87131. Fax: 505-272-6995; E-mail: achigaev@salud.unm.edu.

[2] To whom correspondence may be addressed: MSC08 4630, 915 Camino de Salud, Albuquerque, NM 87131. Fax: 505-272-6995; E-mail: lsklar@salud.unm.edu.

[3] The abbreviations used are: GPCR, guanine nucleotide-binding protein-coupled receptor; ABC, antibody binding capacity, corresponds to a total number of antibody binding sites; fMLFF, *N*-formyl-L-methionyl-L-leucyl-L-phenylalanyl-L-phenylalanine, formyl peptide; FPR, formyl peptide receptor 1; LDV-containing small molecule, 4-((*N*′-2-methylphenyl)ureido)-phenylacetyl-L-leucyl-L-aspartyl-L-valyl-L-prolyl-L-alanyl-L-alanyl-L-lysine); LDV-FITC-containing small molecule (4-((*N*′-2-methylphenyl)ureido)-phenylacetyl-L-leucyl-L-aspartyl-L-valyl-L-prolyl-L-alanyl-L-alanyl-L-lysine-FITC; mAb, monoclonal antibody; MCF, mean channel fluorescence, equivalent of mean fluorescence intensity; VLA-4, very late antigen 4; CD49d/CD29, $\alpha_4\beta_1$ integrin; FITC, fluorescein isothiocyanate; PMA, phorbol 12-myristate 13-acetate; EGF, epidermal growth factor; PE, phycoerythrin.

tion of multiple G-protein-coupled receptors on a single cell creates a plethora of conformational states. Understanding of the relationship between inside-out signaling through GPCRs and integrin conformational regulation will provide valuable insight into the dynamic regulation of cell adhesion.

One technique to study conformational changes of integrins uses conformationally sensitive mAbs that bind to epitopes which are hidden in one conformation and exposed under certain conditions. Lately, it has been accepted that integrins exhibit two major conformations, resting and activated. A number of mAbs for "activated" integrins have been described, and the epitopes have been mapped. Together with mapping of these epitopes into three-dimensional structures of integrin (8), epitope exposure can provide helpful information about integrin conformational changes upon signaling. Moreover, because integrin inside-out activation through different signaling pathways can result in different activation states, the use of previously mapped mAbs can help dissect conformational changes upon activation.

Although it is clear that inside-out activation results in a conformational rearrangement of the integrin molecule, the relationship between affinity state of the ligand binding pocket and overall molecule conformation is still debated. Currently, two contrasting models of integrin inside-out integrin activation are described. The "switchblade" model implies that an open head structure with swung-out β-hybrid domain represents the high (or at least intermediate) affinity state. A feature of this model is that integrin extension provides space for hybrid domain swing. The "deadbolt" model proposes that the movement of β-hybrid domain is not related to the inside-out signal. Ligand binding by itself can provide the energy for the hybrid domain swing out (for details, see Ref. 9 and references therein). Because these two models assign different roles to the hybrid domain motion, we evaluated the exposure of VLA-4 hybrid domain epitopes upon activation through two $G\alpha_i$-coupled GPCRs (FPR and CXCR4) and ligand binding using the conformationally sensitive HUTS-21 mAb with an epitope mapped to the hybrid domain of β1-integrin (10).

We found that contrary to previous reports, where these mAbs were reported to bind or used for the detection of activated integrin (10–13), formyl peptide or SDF-1 treatment alone did not result in any significant exposure of HUTS-21 epitope despite the fact that the VLA-4 affinity up-regulation was detected in parallel on the same batch of cells. Quantitative analysis of mAb binding in real time on live cells suggests that for both the low (resting) and high affinity (induced by inside-out pathway) states, occupancy of the ligand binding pocket rather than inside-out signaling by itself causes the conformational change. Thus, these data support the idea that the hybrid domain movement, which results in the exposure of the mAb epitope, and the high affinity state of the binding pocket are regulated separately and independently of each other, a feature of the deadbolt model of inside-out activation.

EXPERIMENTAL PROCEDURES

Materials—The VLA-4-specific ligand (14–16) 4-((*N*′-2-methylphenyl)ureido)-phenylacetyl-L-leucyl-L-aspartyl-L-valyl-L-prolyl-L-alanyl-L-alanyl-L-lysine (LDV-containing small molecule) and its FITC-conjugated analog (LDV-FITC) were synthesized at Commonwealth Biotechnologies. Mouse anti-human CD29, HUTS-21(PE), PE mouse anti-human CD49d (α_4-integrin subunit, PE) clone 9F10, isotype control (mouse IgG2a κ PE) clone G155–178, isotype control (mouse IgG1 κ PE) clone MOPC-21 were purchased from BD Biosciences and used according to the manufacturer's instructions. Mouse anti-human CD29, clone HUTS-4, was purchased from Millipore Corp. Simply Cellular anti-mouse IgG microspheres were purchased from Bangs Laboratories, Inc. All other reagents were from Sigma-Aldrich. Stock peptide solutions were prepared in DMSO at concentrations ~1000-fold higher than the final concentration. Usually, 1 μl of stock solution was added to 1 ml of cell suspension yielding a final DMSO concentration of 0.1%. Control samples were treated with equal amounts of pure DMSO (vehicle).

Cell Lines and Transfectant Construct—The human histiocytic lymphoma cell line U937 was purchased from ATCC. Site-directed mutants of the FPR (non-desensitizing mutant of FPR ΔST) in U937 cells were prepared as described (17) and were a gift of Dr. Eric Prossnitz (University of New Mexico). High receptor expressing cells were selected using the MoFlo Flow Cytometer (DakoCytomation). Cells were grown at 37 °C in a humidified atmosphere of 5% CO_2 and 95% air in RPMI 1640 (supplemented with 2 mM L-glutamine, 100 units/ml penicillin, 100 μg/ml streptomycin, 10 mM HEPES, pH 7.4, and 10% heat-inactivated fetal bovine serum). Cells were then harvested and resuspended in 1 ml of HEPES buffer (110 mM NaCl, 10 mM KCl, 10 mM glucose, 1 mM $MgCl_2$, 1.5 mM $CaCl_2$, and 30 mM HEPES, pH 7.4) containing 0.1% human serum albumin and stored on ice. The buffer was depleted of lipopolysaccharide by affinity chromatography over polymyxin B Sepharose (Detoxigel; Pierce). Cells were counted using the Coulter Multisizer/Z2 analyzer (Beckman Coulter). For experiments, cells were suspended in the same HEPES buffer at 10^6 cells/ml and warmed to 37 °C for 10 min before real-time binding experiments (see below).

Cell Surface Staining—U937 cells were suspended in the HEPES buffer (see above), 1×10^7 cells/ml, and 100-μl aliquots (10^6 cells) were incubated on ice for 30 min with 20 μl of antibodies. Next, cells were washed with 1 ml of HEPES buffer, resuspended in 300–500 μl of buffer, and analyzed by flow cytometry. To maintain GPCR signaling and VLA-4 conformational change, binding of HUTS-21 antibodies was performed for 30 min at 37 °C.

Real-time Binding of HUTS-21 Antibodies—The ability of a flow cytometer to discriminate between free and bound fluorescent ligand in a homogeneous assay was used to determine binding kinetics of mAbs in real time (18). Cells (10^6 cells/ml) removed from ice were warmed in HEPES buffer containing 0.1% human serum albumin for 10 min at 37 °C. Flow cytometric data were acquired continuously for up to 1024 s at 37 °C, whereas the samples were stirred continuously at 300 rpm with a 5 × 2-mm magnetic stir bar (Bel-Art Products). First, samples were analyzed for 30–120 s to establish a base line for unstained cells marked on figures as "autofluorescence." Next, the tube was removed, HUTS-21 mAbs (20 μl/1 ml of cells) were added, and acquisition was re-established, creating a 5–10-s gap in the

time course. For real-time activation experiments, different stimuli (fMLFF, at saturating concentration (100 nM final), LDV at different concentrations) were added after 60–120 s. Then, acquisition was re-established, and data were acquired continuously for up to 1024 s. For long term kinetic measurements, the tube was removed and incubated at 37 °C, whereas the samples were stirred continuously. Next, single point measurements were taken at different time points, collecting 5,000–10,000 events (see Fig. 1*C*). The resulting data were converted to mean channel fluorescence (MCF) *versus* time using FCSQuery software developed by Dr. Bruce Edwards (University of New Mexico).

Calibration of Surface Markers—Expression of integrin molecules was measured with fluorescent mAbs and quantified by comparison with a standard curve generated with Simply Cellular anti-mouse IgG microspheres (Bangs Laboratories) stained in parallel with the same mAb according to manufacturer instructions. This produces an estimate of the antibody binding capacity (ABC) that corresponds to the total number of mAb binding sites/cell.

Statistical Analysis—Curve fits and statistics were performed using GraphPad Prism Version 4.00 for Windows, GraphPad Software, San Diego, CA. Each experiment was repeated at least three times. The experimental curves represent the mean of two or more independent runs. S.E. was calculated using GraphPad Prism.

Homology Modeling—Homology modeling was used to build two models of the human VLA-4 (open and closed conformation) to generate three-dimensional structures for VLA-4 multiple conformational states, which recently have been visualized for $\alpha_{IIb}\beta_3$ integrin using electron microscopy and x-ray crystallography (19–21). The crystal structure of $\alpha_V\beta_3$ in complex with cyclo(RGDf[NMe]V) ligand (Protein Data Bank code 1L5G) (22, 23) was used as a template to build a three-dimensional model for human VLA-4 integrin in the bent closed conformation. Because 1L5G structure does not offer any structural information regarding EGF-1 and EGF-2, we have modeled these pieces based on EGF-3 and EGF-4 fragments and inserted them between the hybrid and EGF-3 domains. The three-dimensional model for VLA-4 with open headpiece was built using the crystal structure of $\alpha_{IIb}\beta_3$ integrin (Protein Data Bank code 1TXV) as a template (21). The integrin subunit sequences were first aligned by applying the default parameters of T-Coffee package (24, 25), and then they were manually adjusted to align important residues and to avoid insertions or deletions in the conserved regions. The final alignments were submitted for automatic modeling to the SWISS-MODEL server (26–28), and the resulting models were minimized using the Biopolymer module from Sybyl software suite (SYBYL 7.3, Tripos International).

As we expected, by overlapping the headpiece of the two $\alpha_4\beta_1$ models, we observed no significant differences between orientations of the β-propeller in either α_4 subunits. The major structural modification found is the sliding of α7-helix and the swing-out of the hybrid domain in the β_1-subunit. To generate in the next step the intermediate states in equilibrium between known conformational structures of $\alpha_4\beta_1$, we used both β_1-subunits in open and closed conformation and only the α_4-subunit modeled according to the α_V integrin.

RESULTS

Inside-out Activation through FPR or CXCR4 Does Not Result in Significant HUTS-21 Epitope Exposure in the Absence of Integrin Ligand—Binding of HUTS-21 is often presented as a way to assess "activation status" of β_1 integrins (29–31). For several years we have systematically studied the regulation of VLA-4 affinity and conformation using a model system, which consists of U937 cells transfected with a non-desensitizing mutant of FPR (ΔST). All serines and threonines in C-terminal part of this receptor were mutated, and therefore, the receptor cannot be phosphorylated, desensitized, and internalized (32). On resting cells the majority of integrin molecules exhibit a low affinity bent conformation. After activation by formyl peptide, the affinity state is up-regulated, and rapid molecule unbending (extension) can also be detected using a fluorescence resonance energy transfer-based assay. This activated state persists for more than 25–30 min because of the lack of receptor desensitization (4, 14, 16, 33). We took advantage of this well characterized model system to study how HUTS-21 would report this persistent activated state. Surprisingly, very low HUTS-21 binding was detected (Fig. 1*A*, *fMLFF bar*). In a parallel experiment with fluorescent LDV ligand, using the same batch of U937 cells, we detected rapid affinity up-regulation (data not shown and Refs. (4, 14, and 15). The addition of LDV-containing ligand at a saturating concentration induced significant HUTS-21 binding in the absence of activation (Fig. 1*A*, *LDV bar*). Quantitatively, the value of fluorescence attributed to specific binding of HUTS after fMLFF treatment was less than 10% that of the value for the ligand induced conformational change (Fig. 1*A*, compare the values in the *rectangles*). Similar experiments were performed using U937 cells stably transfected with CXCR4 receptor. No significant binding of HUTS-21 after cell treatment with SDF-1 was detected (data not shown). Thus, activation of U937 cells through a non-desensitizing GPCR or CXCR4 in the absence of ligand was insufficient to induce full exposure of HUTS-21 epitope.

Next, to study the kinetics of epitope exposure, we performed a real-time analysis of HUTS-21 binding. This is possible because a flow cytometer can discriminate between free and bound ligand without a wash step (18). The addition of HUTS-21 to U937 cells in real-time resulted in a very rapid nonspecific HUTS-21 binding, which was unchanged during the next 50–60 min (see the *DMSO line* in Fig. 1, *B* and *C*). This result indicates that without additional activation no spontaneous HUTS-21 epitope exposure can be detected. The addition of saturating amounts of formyl peptide and LDV ligand resulted in a rapid exposure of the epitope and induced antibody binding (Fig. 1*B*). However, after fMLFF stimulation, binding of HUTS-21 reached a plateau. The addition of LDV induced sustained long term binding (Fig. 1*C*). Moreover, the ratio between MCF values for LDV-stimulated cells *versus* fMLFF stimulation attributed to the specific binding of HUTS after a long incubation in real-time binding assay without the wash step (428/31 = 13.8) was very similar to the ratio determined in a regular antibody binding assay that includes a wash

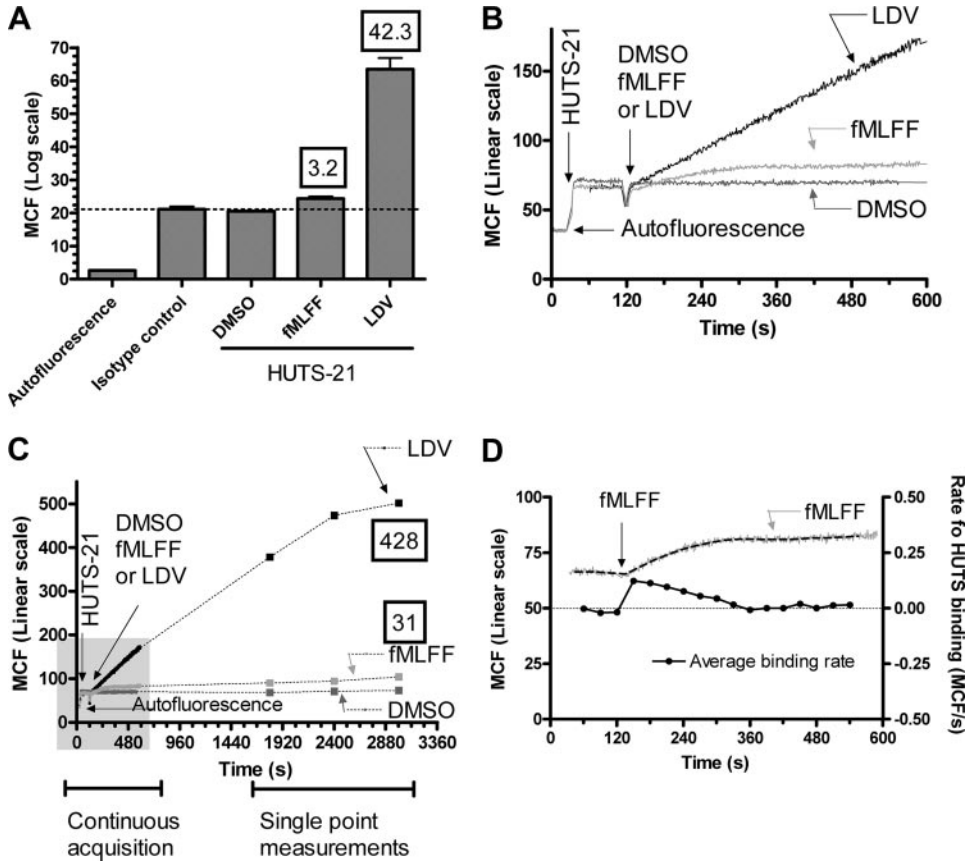

FIGURE 1. **Binding of HUTS-21 antibodies to U937 cells stably transfected with a non-desensitizing mutant of FPR.** *A*, cells were incubated for 40 min at 37 °C in the presence of isotype control or HUTS-21 antibody and different activation stimuli: DMSO (control), fMLFF (100 nM), LDV (1 μM). Next, cells were washed, and red fluorescence was measured (FL2); see "Experimental Procedures" for details. Each *bar* represents the mean ± S.E. of three independent determinations ($n = 3$). *B*, real-time binding of HUTS-21 antibodies after activation through FPR. Experiments were performed as described under "Experimental Procedures." Cells were treated with HUTS-21 mAbs, DMSO (vehicle), LDV (1 μM), or fMLFF (100 nM). The addition of HUTS-21 antibodies (*first arrow*) resulted in a rapid nonspecific binding of antibodies. Without ligand addition no additional binding was detected (DMSO). The addition of a saturating amount of the LDV ligand (*second arrow*) led to progressive antibody binding over a long time. Cell activation by fMLFF did not significantly affect binding in the absence of the ligand. *C*, the same experiment as shown on a *panel B*, extended for a longer time. Tubes were removed and incubated for additional time. Single point measurements were made. The area corresponding to a *panel B* (continuous acquisition) is indicated by *gray shading* on *panel C*. *D*, kinetics of HUTS-21 epitope exposure after cell activation through FPR. Average binding rates of MCF change (measured in MCF per second) were calculated for each 30-s time interval and plotted on Fig. 1*D* (*right y* axis) together with a line showing HUTS-21 binding (left *y* axis, analogous to fMLFF line on Fig. 1, *B* and *C*).

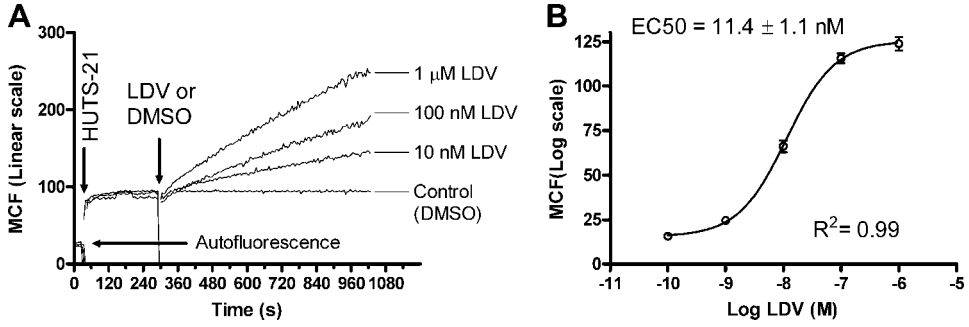

FIGURE 2. **LDV concentration-dependent binding of HUTS-21 to resting cells (without FPR activation).** *A*, kinetics of real-time binding of HUTS-21 antibodies to U937 cells. The addition of HUTS-21 antibodies (*first arrow*) resulted in rapid nonspecific binding of antibodies. The addition of increasing amounts of LDV ligand resulted in the different rates of antibody binding (compare slopes after LDV additions). *B*, binding of HUTS-21 plotted *versus* LDV concentration. Cells were incubated with the indicated concentrations of LDV in the presence of an excess of HUTS-21 mAbs and washed, and MCF was measured. Each point represents the mean ± S.E. of three independent determinations ($n = 3$). The data were fitted using the sigmoidal dose-response equation with variable slope using GraphPad Prism software (the HillSlope was found to be ~1). A representative experiment of three independent experiments is shown.

step (42.3/3.2 = 13.2). Thus, two different assays provide very similar results.

To study the kinetics of epitope exposure after FPR activation, we calculated absolute rates of HUTS-21 binding after the addition of fMLFF. The rate of HUTS binding reached its maximal value during the first 30 s after fMLFF addition. Three and half minutes later HUTS-21 binding stopped. Thus, these data indicate that HUTS-21 epitope is only exposed in the first 4 min after inside-out signaling was initiated by the addition of GPCR ligand. This result was not anticipated because cells are transfected with a non-desensitizing mutant of FPR, and the VLA-4 receptor is reported to maintain a high affinity unbent conformation for at least 20–30 min after the addition of fMLFF (4, 7, 14–16). Thus, in the absence of the integrin ligand, the HUTS-21 epitope is exposed for a very short period of time after cell activation. The data suggest that the occupancy of the ligand binding site rather than inside-out activation *per se* is necessary for HUTS-21 epitope exposure.

Occupancy of the Ligand Binding Site in the Absence of Integrin Activation Is Sufficient to Induce HUTS Epitope Exposure—To find out how occupancy of the ligand binding site affects HUTS-21 binding, we have studied HUTS-21 binding at different concentrations of LDV ligand (Fig. 2). The addition of different concentrations of LDV resulted in a different rates of HUTS-21 binding (Fig. 2*A*). Long term incubation of U937 cells with a large excess of HUTS-21 in the presence of different concentrations of LDV (Fig. 2*B*) resulted in a sigmoidal binding curve. The EC_{50} for HUTS-21 binding in this case (EC_{50} = 11.4 nM) is identical to a previously published K_d for binding of LDV-FITC to resting U937 cells ($K_d \sim 12$ nM) (14). Thus, in the absence of cell activation, LDV to the VLA-4 integrin induces HUTS-21 epitope exposure detected by HUTS-21 binding. Because the EC_{50} for HUTS-21

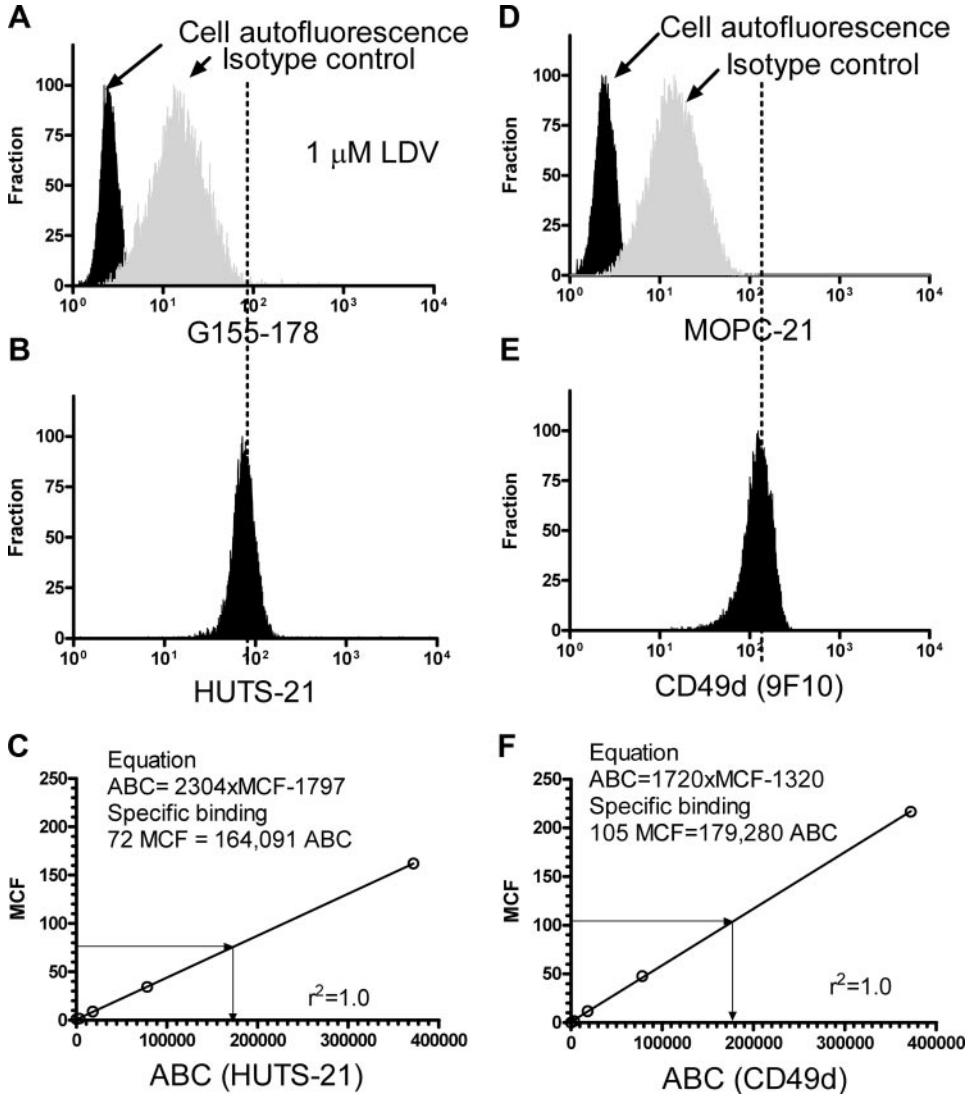

FIGURE 3. **Estimation of number of HUTS-21 and anti-CD49d (9F10, anti α4-integrin) mAbs binding sites on U937 cells.** Cells were incubated with isotype control, HUTS-21, or 9F10 (see the "Experimental Procedures" for details). *A*, histograms for cell autofluorescence and isotype control (G155–178, isotype control for HUTS-21). *B*, histogram for HUTS-21 binding. *C*, calibration curve generated using Simply Cellular anti-mouse IgG microspheres for HUTS-21 mAbs. *D*, histograms for cell autofluorescence and isotype control (MOPC-21, isotype control for 9F10). *E*, histogram for 9F10(anti-CD49d) binding. *F*, calibration curve generated using Simply Cellular anti-mouse IgG microspheres for 9F10 (anti-CD49d) mAbs. Equations and calculated ABCs are shown in *panels C* and *F*. The difference in the ABC values for HUTS-21 and CD49d was not statistically significant.

binding induced by the binding of LDV is equivalent to the K_d for ligand binding in the absence of HUTS-21, these data also confirm that binding of HUTS-21 to the β_1-integrin subunit had no effect upon affinity of LDV ligand binding.

Induction of HUTS-21 epitope by LDV ligand can be also observed on ice (data not shown), suggesting that no intracellular signaling is involved in this type of conformational change. Thus, it is possible that ligand binding by itself "mechanically" induces a series of conformational changes (for example, see Fig. 7 in Ref. 34) leading to the exposure of the epitope.

The Number of Bound HUTS-21 Corresponds to the Total Number of CD49d Binding Sites—Next, to quantify the number HUTS-21 binding sites on U937 cells, we used Quantum Simply Cellular beads (Bangs Laboratories) to calibrate antibody binding. Cells were saturated with HUTS-21 in the presence of a saturating amount of LDV ligand (1 μM) (Fig. 3). In parallel, cells were stained with anti-CD49d (α_4-integrin subunit) antibodies. Simply Cellular beads were saturated with the same antibodies. This resulted in two calibration lines that were used to estimate ABCs (Fig. 3, *C* and *F*). The data showed that the numbers of bound HUTS-21 (ABC ~ 164,000) and anti-CD49d (ABC ~ 179,000) were very similar, indicating that essentially every VLA-4 molecule can adopt a conformation with exposed HUTS-21 epitope after LDV ligand binding. As shown previously, the number of VLA-4 molecules detected on U937 cells is similar to the number of fluorescent LDV-FITC molecules bound to U937 cells (14). Therefore, the number of VLA-4 sites with bound HUTS-21 corresponds to the number of sites occupied by the ligand.

The Rate of HUTS-21 Binding Can Be Used to Determine Integrin Affinity State—According to our data, binding of HUTS-21 can be described in the following simple model,

$$L + R \underset{k_{-1}}{\overset{k_{+1}}{\longleftrightarrow}} LR \qquad \text{(Eq. 1)}$$

$$LR + HUTS \xrightarrow{k_{+2}} (LR \cdot HUTS) \qquad \text{(Eq. 2)}$$

where *L* is the concentration of LDV ligand, R is the concentration of VLA-4 receptor, and LR is the concentration of ligand-receptor complex. HUTS is the concentration of HUTS antibodies, and LR·HUTS is the concentration of HUTS bound to ligand-occupied VLA-4. Because flow cytometers have the ability to discriminate between free and bound fluorescent ligand in a homogeneous assay (18), MCF is proportional to LR·HUTS. In the absence of LDV ligand, no ligand receptor complex is formed, and therefore, no binding of HUTS-21 is observed (Fig. 1, *B* and *C*, *DMSO line*). The addition of different concentrations of LDV results in the formation of the ligand-receptor complex, and this is reflected in the different rates of HUTS-21 binding (Figs. 2*A* and 4*A*). Because binding of a large antibody molecule is limited by diffusion, antibody binding is slow compared with the binding of a small LDV molecule. Also on this time scale binding of antibodies is virtually irreversible (Equation 2). The ligand equilibration time (and approach to equilib-

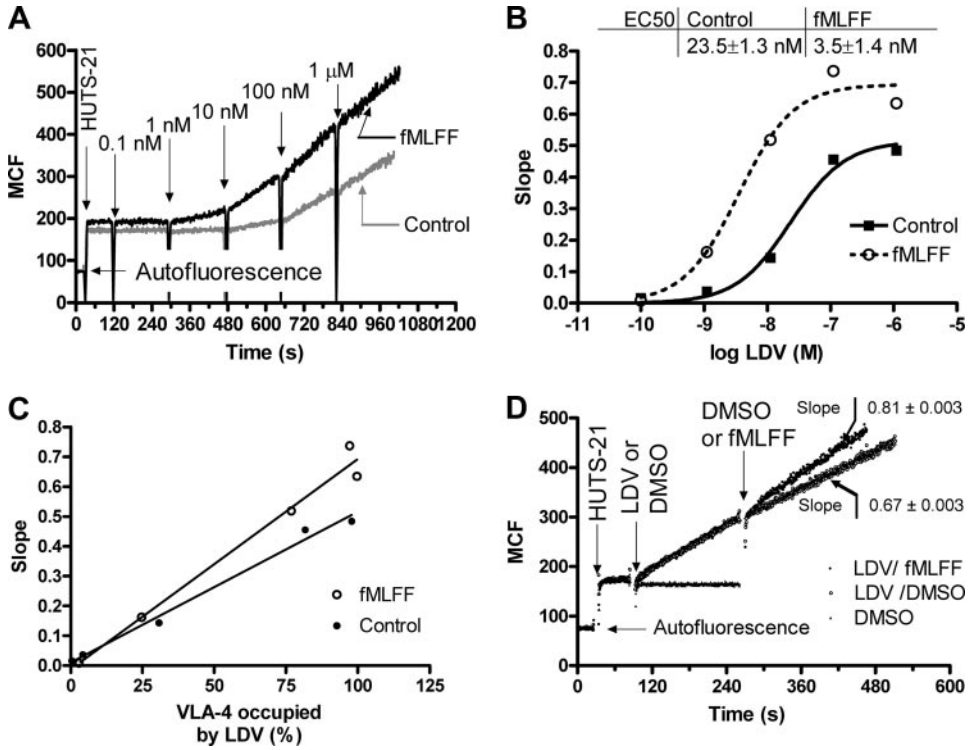

FIGURE 4. **Kinetics of real-time binding of HUTS-21 antibodies to U937 cells, transfected with a non-desensitizing mutant of formyl peptide receptor.** *A*, cells were treated with 100 nM of fMLFF (activated) or DMSO (vehicle) 5 min before the start of the experiment. The addition of HUTS-21 antibodies (*first arrow*) resulted in a rapid nonspecific binding of the antibody. Next, increasing amounts of LDV ligand were added. This induced binding of mAbs and resulted in different rates of antibody binding (compare slopes after LDV additions). *B*, absolute rates HUTS-21 binding (slopes of lines between sequential LDV additions calculated from *panel A*) plotted *versus* concentration of LDV in solution. The fit to the data was done using the sigmoidal dose-response equation with variable slope using GraphPad Prism software. Difference in EC_{50} values for resting and activated cells indicated the affinity change for LDV binding. A representative experiment of three independent experiments is shown. *C*, the slopes of the lines between sequential LDV additions, calculated from *panel A*, are plotted *versus* the fraction of VLA-4 occupied by LDV. The fraction of VLA-4 occupied by LDV was calculated using the one-site binding equation ($Y = 100 \times LDV/K_d + LDV$, where *Y* is % of sites occupied, LDV is LDV concentration, and K_d is a previously published dissociation constant for resting and fMLFF activated states). *D*, the change in the rates of HUTS-21 binding can be seen in real-time. Cells pretreated with HUTS-21 antibodies (*first arrow*) were treated with a very high saturating concentration of LDV (10 μM, *second arrow*). Next, cells were activated by fMLFF. Control samples (DMSO) are also shown. Despite the fact that VLA-4 is completely saturated by LDV (10 μM is ~1000-fold higher than K_d), the change in the slope of the line indicating HUTS-21 binding can be detected. A representative experiment of three independent experiments is shown.

rium) is determined by its dissociation rate constant (k_{-1}). For the LDV ligand, k_{-1} varies from 0.1–0.06 s^{-1} for the resting state to 0.02–0.01 s^{-1} for fMLFF-activated state (14, 15). Therefore, for these affinity states (resting and fMLFF activated) equilibrium is reached within a few minutes after ligand addition (see Refs. 14 and 15 for real-time LDV-FITC binding kinetics). Binding of HUTS-21 on this time scale is very far from equilibrium (see Fig. 1*C*), and therefore, binding of HUTS is represented by a series of straight lines (Figs. 2*A* and 4*A*). Thus, under these conditions, the binding rate of HUTS-21 is determined by the amount of LR at each time (Equations 1 and 2). Therefore, the observed rate of HUTS-21 binding (the slope of the line, Figs. 2*A* and 4*A*) is proportional to the concentration of ligand receptor complex at each time.

Consecutive addition of increasing amounts of LDV ligand resulted in different rates of HUTS-21 binding (Fig. 4*A*). For each LDV concentration (between LDV additions) absolute rates of HUTS-21 binding were determined by fitting to the linear regression equation. Next, the slope of each line was plotted *versus* LDV concentration for every time interval (see Fig. 4*B*). This resulted in a sigmoidal dose-response curve that shows the relationship between the concentration of exposed HUTS-21 epitope and the concentration of LDV in solution. Experiments were performed without significant ligand depletion, because the total concentration of VLA-4 receptors in solution was <0.3 nM (~170,000 molecules/cell (Fig. 3), 10^6 cells/ml). Both EC_{50} values for the resting and fMLFF-activated cells were comparable with previously published K_d values for the binding of LDV-FITC to U937 cells (14, 15). Thus, binding of the ligand depends upon its concentration and the affinity of the VLA-4 receptor (activation state of the integrin). A combination of these two factors determines (LR) (see Equations 1 and 2) and thereby drives HUTS-21 binding.

The Rate of HUTS-21 Binding Appears to Be Related to Inside-out Activation through FPR—A thorough examination of antibody binding rates revealed another intriguing phenomenon. Absolute rates of HUTS-21 binding to U937 cells activated by fMLFF were faster than the binding rates for the resting cells at the same fraction of ligand occupied receptors (Fig. 4*C*). This effect was not related to the phenomenon described in Fig. 1*D* because fMLFF was added 5 min before the start of the experiment (see the legend to Fig. 4). No significant binding HUTS-21 was detected in the absence and at low concentration of LDV ligand. The initial slope after the addition of HUTS-21 was horizontal for up to 300 s (see Fig. 4*A*). An increase in the rate of HUTS-21 binding can be also seen in real-time under the condition that VLA-4 was completely saturated with LDV ligand (Fig. 4*D*). The LDV ligand concentration in this experiment was ~10 μM, which is about 1000-fold higher than the K_d for LDV binding at this affinity state (K_d ~ 12 nM (14)). The simplest interpretation is that the activation of integrin through GPCR results in a conformational change which increases the rate of HUTS-21 binding. As shown previously, inside-out activation of integrins results in up-regulation of ligand binding affinity and unbending (extension) of the integrin molecule. The affinity change and unbending represent two different conformational changes that are regulated independently by different signaling pathways (4). Thus, we propose that an increase in the rate of HUTS-21 binding could be attributed to the unbending (extension) of the molecule induced by inside-out activa-

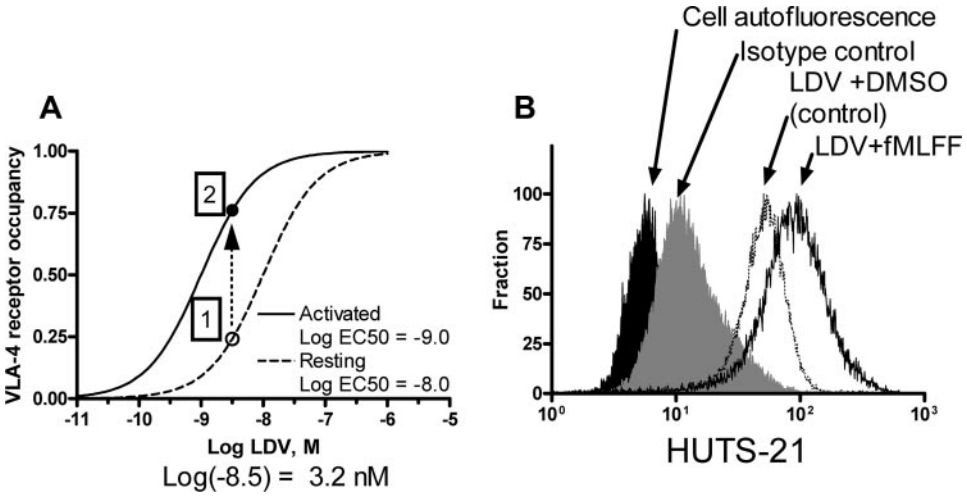

FIGURE 5. **Detection of high affinity state of VLA-4 using HUTS-21 antibodies.** *A*, simulation of LDV binding for two affinity states of VLA-4 performed using a sigmoidal dose-response binding equation ($Y = 1/(1 + 10^{(\log EC_{50} - X)})$, where Y is receptor occupancy, and X is the log of LDV concentration). EC_{50} values for resting and activated states are indicated. The maximal difference receptor occupancy for low and high affinity states was determined by subtracting the resting curve from the activated curve on a point by point basis. The maximal difference was observed at log −8.5 = 3.2 nM of LDV in solution. The *arrow* indicates additional binding of LDV ligand at 3.2 nM from low affinity receptor state (*point 1*) to a high affinity receptor state (*point 2*). *B*, experimental data showing additional binding of HUTS-21 antibodies induced by fMLFF activation in the presence of 3.2 nM LDV. Histograms for cell autofluorescence, isotype control, low affinity state (LDV + DMSO), and high affinity state (LDV + fMLFF) are shown. Each histogram represents a mean of three independent determinations ($n = 3$). A representative experiment of three independent experiments is shown.

tion. It is also possible that inside-out activation would increase the probability of a hybrid domain movement (for example, by changing the overall "flexibility" of the molecule) and thereby augment the overall concentration of the exposed epitope in solution. Other possibilities include a conformational change that is not related to the extension of the molecule.

Next, to test the proposition that an increase in the rate of HUTS-21 binding is related to integrin unbending (extension), we treated cells with phorbol ester (PMA). Previously, we showed that this type of activation results in the high affinity state of the VLA-4 ligand binding pocket, which occurred without molecule unbending (extension) (see Fig. 2 in Ref. 4). No significant change in the rate of HUTS-21 binding was detected after cells were activated with PMA in experiments analogous to Fig. 4*D* (data not shown). This also supports the idea that integrin extension facilitates HUTS-21 binding and, thus, increases the binding rate.

HUTS-21 Can Be Used to Detect the Activated (High Affinity) State of VLA-4—Previously we established a simple method for the detection of VLA-4 affinity change in real time on live cells (14). A transition from low to high affinity state leads to additional binding of the LDV-FITC probe if cells were preincubated with the ligand at concentrations below the K_d for the low affinity state and above the K_d for the high affinity state. In the case of a fluorescent ligand this additional binding can be detected using a conventional flow cytometer in a homogeneous assay (4, 14, 15). Our present data show that binding of HUTS-21 antibodies can be used as a reporter of a ligand-occupied receptor (see Fig. 2*B*). Therefore, detection of the high affinity state of VLA-4 can be performed with an unlabeled ligand and HUTS-21. To determine the concentration where the biggest difference in the ligand binding after activation will be observed, we generated two theoretical binding curves (Fig. 5). Next, we have determined that at 3.2 nM (log −8.5) VLA-4 receptor occupancy would increase from ~0.24 to ~0.76 after the affinity change (*arrow*, Fig. 5*A*). The experiment, where HUTS-21 binding occurred in the presence of 3.2 nM LDV, showed a significant difference between resting and fMLFF-activated cells (Fig. 5*B*, compare LDV + DMSO (control) with LDV + fMLFF). Thus, in the presence of properly chosen concentration of the ligand (~3.2 nM for LDV), binding of HUTS-21 is also sensitive to cellular activation status.

Binding of HUTS-21 may be complicated if the assay is performed in the presence of serum containing soluble integrin ligands. In our experiments the addition of heat-inactivated fetal bovine serum induced a dose-dependent binding of HUTS-21 without any additional activation. Activation through the FPR resulted in a larger signal (data not shown).

DISCUSSION

In a thoroughly characterized model system, using the conformationally sensitive mAb HUTS-21, a VLA-4-specific ligand with known affinity and binding kinetics, we studied the effect of inside-out activation upon HUTS-21 epitope exposure on live cells in real time. We also investigated how the occupancy of the ligand binding pocket affected VLA-4 conformation at different affinity states. We found that (i) in the absence of ligand, activation by FPR or CXCR4 did not result in a significant exposure of the HUTS-21 epitope, (ii) ligand binding alone was sufficient to instantaneously induce HUTS-21 epitope exposure, (iii) quantitatively the number of ligand-occupied receptors was similar to the number of bound HUTS-21, and (iv) binding of HUTS-21 was determined by the affinity state of VLA-4 receptor and the concentration of the ligand. Binding of HUTS-21 reports the high affinity-activated state of the VLA-4 only in the presence of properly chosen ligand concentration. Taken together with previously published data this suggests that affinity state and HUTS-21 epitope exposure are regulated through different mechanisms. On this basis, we propose a model of integrin conformational regulation.

Exposure of HUTS Epitope and Integrin Conformational Changes—HUTS is a group of three mAbs (HUTS-4, HUTS-7, and HUTS-21) that recognize overlapping epitopes on β_1-integrin subunit (CD29) mapped to 355–425-amino acid-residue β_1-integrin polypeptide. Binding of these mAbs also was shown to be functionally identical, *e.g.* they exhibited the same binding pattern upon integrin activation using different activation stimuli (EGTA, divalent ions, and temperature dependence) (10).

The sequence 355–425 lies within the β_1-subunit hybrid domain, and HUTS-4 epitope was fine-mapped to Ser^{370}, Glu^{371}, and Lys^{417} (34). Because of the proximity of the hybrid domain to the β-propeller of the integrin α-subunit, the HUTS-4 epitope can be masked, thereby preventing mAb binding. A conformational change that involves a movement of α7 helix and outward swing (also called swing-out) of the hybrid domain is argued to be necessary for the epitope exposure (see Fig. 7 in Ref. 34 or Fig. 6 in Ref. 35).

In the current work we took advantage of commercially available HUTS-21 mAbs, which have a similar to HUTS-4 binding pattern before and after cell activation and cross-compete with HUTS-4 mAbs (Ref. 10 and data not shown). This suggests that HUTS-4 and HUTS-21 epitopes are very close, and therefore, these antibodies detect similar types of conformational changes.

Inside-out Activation of Integrin and Hybrid Domain Swing-out—According to Arnaout *et al.* (9), two existing models of integrin inside-out activation (switchblade model and deadbolt model) imply different roles for the hybrid domain swing-out. The switchblade model puts forward the idea that the structure with a swung-out hybrid domain represents a high (or at least intermediate) affinity state. Swinging away the hybrid domain pulls on the C-terminal α-helix of β I-like domain (βA domain). This converts the low affinity binding pocket to the high affinity state (see Fig. 12*A* in Ref. 36). Thus, according to the switchblade model, the hybrid domain swing-out is necessary for integrin conformational activation. The deadbolt model proposes that the hybrid domain swing-out is an attribute of the outside-in signaling pathway. It is argued that binding of the ligand by itself rather than a conformational change induced by inside-out signaling pathway "provides the energy" required for a swing-out motion (9).

Current data provide valuable insight into the mechanism of integrin conformational regulation. Activation of U937 cells through a non-desensitizing mutant of FPR results in the high affinity state of the VLA-4 ligand binding pocket, which persists for more than 1000 s (4, 14, 33). In this case the absence of a major HUTS-21 epitope exposure suggests that hybrid domain swing-out is not directly related to the induction of the high affinity state. Given that it is impossible to measure ligand affinity in the absence of the ligand itself, this conclusion is debatable. However, the current paradigm implies that the high affinity state of the integrin binding pocket is generated as a result of conformational changes in response to inside-out activation and exists before the ligand binding (9, 19, 36). Moreover, in previous work, no ligand-induced affinity changes were detected in our model system in response to LDV probe binding alone. Thus, our data suggest that after inside-out activation through GPCR, VLA-4 assumes a high affinity conformation with the HUTS-21 epitope remaining hidden.

Moreover, incubation of U937 cells with different LDV ligand concentrations showed that HUTS-21 binding reflects ligand binding affinity (EC_{50} values for HUTS-21 binding are identical to the K_d values for LDV ligand binding for both resting and FPR activated states (14, 15)). Taken together these data suggest that the affinity state and HUTS-21 epitope exposure are regulated independently (Fig. 6). However, the affinity state

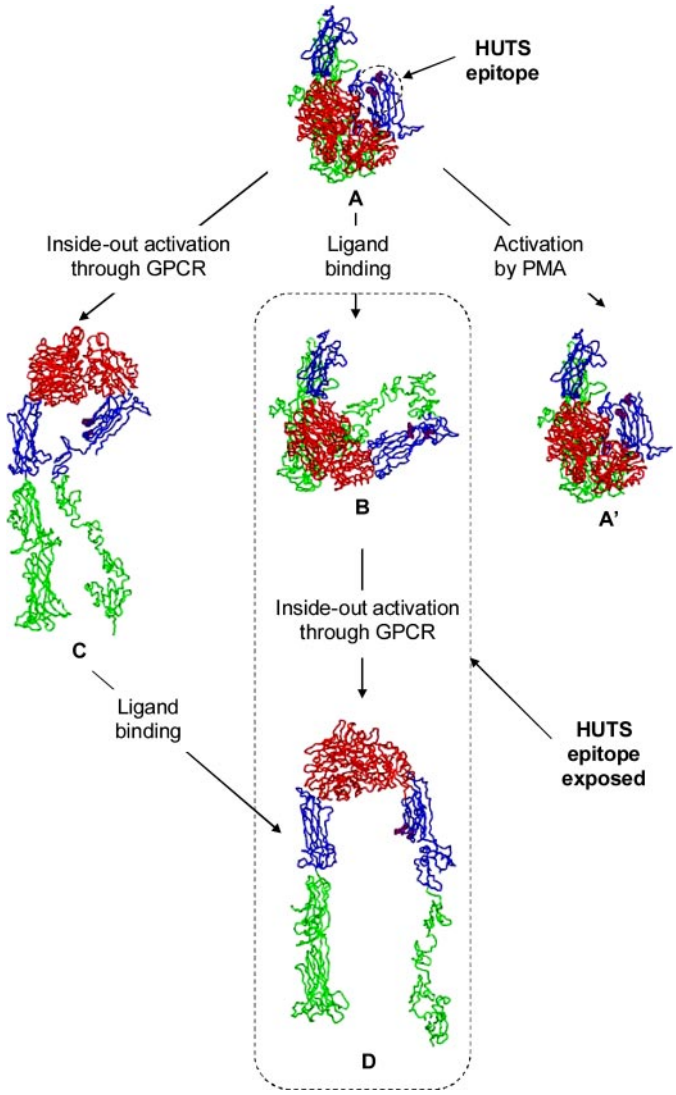

FIGURE 6. **Model of integrin conformations.** Three-dimensional structures for VLA-4 multiple conformational states have been generated as described under "Experimental Procedures" by combining the integrin structural information existent in Protein Data Bank and relevant literature data (21, 22). The integrin head is colored in *red*, the "upper legs" are in *blue*, and the "lower legs" are in *green*. In the model Ser^{370}, Glu^{371}, and Lys^{417}, which represent HUTS epitope (34), are shown by *purple space fill*. The VLA-4 bent closed conformation is modeled based on crystal structure of $\alpha_V\beta_3$ integrin (structure A). Structure A represents a bent low affinity state (resting state), having the HUTS-21 epitope unexposed (*purple spheres*). As in the template, the N termini of α and β subunits are set into an ovoid-like arrangement from which two parallel tails come out. Because the crystal structure does not offer any structural information regarding EGF-domains, no EGF domains are shown on *A* and *A'* (see the "Experimental Procedures" for details). The conformational change induced by the occupancy of the ligand pocket (structure B) was modeled in two steps. First, the β_1 structure built based on the β_3 open headpiece was translated into the structure A coordinate system. By overlapping the 1L5G (closed bent conformation) and 1TXV (open conformation) structures, we found that the distance between C termini domains of α and β subunits is ~15 Å, and the distance between α and β "knees" is ~70 Å. These constraints were used to build the bent open conformation of VLA-4 (structure B). This structure has the outward swing of the hybrid domain, which causes the exposure of HUTS-21 epitope and represents the low affinity state of the integrin. The unbent conformation with closed and open headpiece (structure C and D, respectively) have been obtained by adjusting the torsion angles at the knees of α4 and β_1 subunits in A and B structures. In these operations the upper and lower legs of each subunit were considered as two rigid systems. All final conformations have been minimized with the Biopolymer module from Sybyl (SYBYL 7.3, Tripos International).

of the ligand binding pocket directly affects ligand binding, which can be reflected in HUTS-21 epitope exposure. Thus, the data oppose the idea that the conformation with exposed hybrid domain represents the activated high affinity state and support the ligand-induced, potentially outside-in role of a hybrid domain swing.

Activation of VLA-4 and Relationship between Affinity, Swing-out of the Hybrid Domain, and Unbending—For a number of years we have studied regulation of VLA-4 conformational activation. We developed methods for monitoring affinity changes and molecular unbending in real-time on live cells. Here, we used the same cells and ligand to study HUTS-21 epitope exposure. At this point we can combine current data with previously published observations to describe the emerging relationship between different VLA-4 conformational states (Fig. 6).

We found that binding of LDV ligand does not cause VLA-4 molecule unbending or at least full (maximal) unbending. This conclusion is based upon the data obtained in a fluorescence resonance energy transfer-based extension assay. In the presence of a high concentration of LDV-FITC (100 nM), an unquenching of the fluorescence resonance energy transfer signal, which is interpreted as molecular unbending, can be detected after activation thorough several GPCRs, Mn^{2+}, reducing agents, Ca^{2+} ionophore, etc. (4, 16, 33). At the same time, the low affinity state of VLA-4 (or at least the lowest affinity state that we have ever seen) can be detected on resting U937 cells even in the presence of a saturating amount of LDV ligand. The affinity can be up-regulated by more than 2 orders of magnitude using different activating agents (14). Also, in the presence of 100 nM LDV, ~91% of the total number of VLA-4 molecules was occupied by HUTS-21 (Fig. 2*B*). These data suggest that the bent low affinity conformation with exposed HUTS-21 epitope may exist on resting cells in the presence of saturating concentration of the ligand (Fig. 6*B*).

Phorbol esters induce the high affinity state of the VLA-4 binding pocket. Quantitatively, the PMA induced state is similar to the state induced by the FPR (inside-out) signaling pathway. However, the absence of fluorescence resonance energy transfer signal change and slow initial rate of cell aggregation suggest that no molecular unbending occurred after PMA activation (see Figs. 2 and 9 in Ref. 4). Similarly to the activation through FPR or CXCR4, treatment of U937 with PMA without LDV ligand present did not result in any significant exposure of HUTS-21 epitope (data not shown). Thus, the high affinity bent conformation can exist without hybrid domain swing-out (Fig. 6*A*). This conformation is tentatively shown as identical to the resting low affinity bent conformation (Fig. 6*A′*). However, structural features which represent this high affinity, unliganded bent conformation after cell activation by phorbol esters remain unidentified.

Inside-out activation induces the high affinity and unbent (extended) state of VLA-4 (4, 14, 16, 33). However, without ligand present, inside-out activation did not result in a major exposure of the HUTS-21 epitope (Fig. 1). An unbent high affinity state without hybrid domain swing-out is a plausible representation (Fig. 6*C*). Because cell activation before the addition of the ligand facilitates enhanced HUTS-21 binding (Fig. 4), it is possible that the unbent conformation with exposed HUTS-21 epitope (Fig. 6*D*) results in more favorable antibody binding than the bent conformation (Fig. 6*B*).

Taken together, these data suggest several different and completely independent regulation mechanisms for integrin affinity state, unbending, and exposure of the HUTS-21 epitope. For affinity state and unbending, these result from two related but different inside-out signaling pathways (4); for the hybrid domain swing-out, it is a conformational change related to the occupancy of the ligand binding pocket. Binding of HUTS-21 reflects a ligand induced binding site. Whereas we previously identified four potential states (low affinity bent, high affinity extended, low affinity extended, high affinity bent), the addition of ligand, which induces the hybrid domain swing-out, leads to the possibility of eight distinct physiological integrin states.

Acknowledgments—We thank Eric R. Prossnitz for providing U937 cells and plasmids and Bruce S. Edwards for providing FCSQuery software.

REFERENCES

1. Johnston, B., and Butcher, E. C. (2002) *Semin. Immunol.* **14,** 83–92
2. Alon, R., and Feigelson, S. (2002) *Semin. Immunol.* **14,** 93–104
3. Alon, R., Kassner, P. D., Carr, M. W., Finger, E. B., Hemler, M. E., and Springer, T. A. (1995) *J. Cell Biol.* **128,** 1243–1253
4. Chigaev, A., Waller, A., Zwartz, G. J., Buranda, T., and Sklar, L. A. (2007) *J. Immunol.* **178,** 6828–6839
5. Salas, A., Shimaoka, M., Kogan, A. N., Harwood, C., von Andrian, U. H., and Springer, T. A. (2004) *Immunity* **20,** 393–406
6. Askari, J. A., Buckley, P. A., Mould, A. P., and Humphries, M. J. (2009) *J. Cell Sci.* **122,** 165–170
7. Chigaev, A., Waller, A., Amit, O., and Sklar, L. A. (2008) *BMC. Immunol.* **9,** 26
8. Humphries, M. J., Symonds, E. J., and Mould, A. P. (2003) *Curr. Opin. Struct. Biol.* **13,** 236–243
9. Arnaout, M. A., Goodman, S. L., and Xiong, J. P. (2007) *Curr. Opin. Cell Biol.* **19,** 495–507
10. Luque, A., Gomez, M., Puzon, W., Takada, Y., Sanchez-Madrid, F., and Cabanas, C. (1996) *J. Biol. Chem.* **271,** 11067–11075
11. Barthel, S. R., Annis, D. S., Mosher, D. F., and Johansson, M. W. (2006) *J. Biol. Chem.* **281,** 32175–32187
12. Caloca, M. J., Zugaza, J. L., Vicente-Manzanares, M., Sanchez-Madrid, F., and Bustelo, X. R. (2004) *J. Biol. Chem.* **279,** 20435–20446
13. Gutierrez-Lopez, M. D., Ovalle, S., Yanez-Mo, M., Sanchez-Sanchez, N., Rubinstein, E., Olmo, N., Lizarbe, M. A., Sanchez-Madrid, F., and Cabanas, C. (2003) *J. Biol. Chem.* **278,** 208–218
14. Chigaev, A., Blenc, A. M., Braaten, J. V., Kumaraswamy, N., Kepley, C. L., Andrews, R. P., Oliver, J. M., Edwards, B. S., Prossnitz, E. R., Larson, R. S., and Sklar, L. A. (2001) *J. Biol. Chem.* **276,** 48670–48678
15. Chigaev, A., Zwartz, G., Graves, S. W., Dwyer, D. C., Tsuji, H., Foutz, T. D., Edwards, B. S., Prossnitz, E. R., Larson, R. S., and Sklar, L. A. (2003) *J. Biol. Chem.* **278,** 38174–38182
16. Chigaev, A., Buranda, T., Dwyer, D. C., Prossnitz, E. R., and Sklar, L. A. (2003) *Biophys. J.* **85,** 3951–3962
17. Kew, R. R., Peng, T., DiMartino, S. J., Madhavan, D., Weinman, S. J., Cheng, D., and Prossnitz, E. R. (1997) *J. Leukoc. Biol.* **61,** 329–337
18. Sklar, L. A., Edwards, B. S., Graves, S. W., Nolan, J. P., and Prossnitz, E. R. (2002) *Annu. Rev. Biophys. Biomol. Struct.* **31,** 97–119
19. Takagi, J., Petre, B. M., Walz, T., and Springer, T. A. (2002) *Cell* **110,** 599–611
20. Takagi, J., Strokovich, K., Springer, T. A., and Walz, T. (2003) *EMBO J.* **22,** 4607–4615
21. Xiao, T., Takagi, J., Coller, B. S., Wang, J. H., and Springer, T. A. (2004) *Nature* **432,** 59–67

22. Xiong, J. P., Stehle, T., Diefenbach, B., Zhang, R., Dunker, R., Scott, D. L., Joachimiak, A., Goodman, S. L., and Arnaout, M. A. (2001) *Science* **294,** 339–345
23. Xiong, J. P., Stehle, T., Zhang, R., Joachimiak, A., Frech, M., Goodman, S. L., and Arnaout, M. A. (2002) *Science* **296,** 151–155
24. Notredame, C., Higgins, D. G., and Heringa, J. (2000) *J. Mol. Biol.* **302,** 205–217
25. Poirot, O., O'Toole, E., and Notredame, C. (2003) *Nucleic Acids Res.* **31,** 3503–3506
26. Arnold, K., Bordoli, L., Kopp, J., and Schwede, T. (2006) *Bioinformatics* **22,** 195–201
27. Guex, N., and Peitsch, M. C. (1997) *Electrophoresis* **18,** 2714–2723
28. Schwede, T., Kopp, J., Guex, N., and Peitsch, M. C. (2003) *Nucleic Acids Res.* **31,** 3381–3385
29. Escudero, E., Martin, A., Nieto, M., Nieto, E., Navarro, E., Luque, A., Cabanas, C., Sanchez-Madrid, F., and Mampaso, F. (2000) *J. Am. Soc. Nephrol.* **11,** 1075–1084
30. Lorentz, A., Schuppan, D., Gebert, A., Manns, M. P., and Bischoff, S. C. (2002) *Blood* **99,** 966–972
31. Luque, R., Garcia-Trujillo, J. A., Camara, C., Moreno, A., Eiras, P., Roy, G., Villar, L. M., Lombardia, M., Brieva, J. A., Bootello, A., and Roldan, E. (2002) *Br. J. Haematol.* **119,** 70–78
32. Hsu, M. H., Chiang, S. C., Ye, R. D., and Prossnitz, E. R. (1997) *J. Biol. Chem.* **272,** 29426–29429
33. Chigaev, A., Zwartz, G. J., Buranda, T., Edwards, B. S., Prossnitz, E. R., and Sklar, L. A. (2004) *J. Biol. Chem.* **279,** 32435–32443
34. Mould, A. P., Barton, S. J., Askari, J. A., McEwan, P. A., Buckley, P. A., Craig, S. E., and Humphries, M. J. (2003) *J. Biol. Chem.* **278,** 17028–17035
35. Mould, A. P., Travis, M. A., Barton, S. J., Hamilton, J. A., Askari, J. A., Craig, S. E., Macdonald, P. R., Kammerer, R. A., Buckley, P. A., and Humphries, M. J. (2005) *J. Biol. Chem.* **280,** 4238–4246
36. Takagi, J., and Springer, T. A. (2002) *Immunol. Rev.* **186,** 141–163